PNAS RESEARCH ARTICLE | BIOPHYSICS AND COMPUTATIONAL BIOLOGY OPEN ACCESS

Conservation of kinetic stability, but not the unfolding mechanism, between human transthyretin and a transthyretin-related enzyme

Marcus Jäger[a,1], Jeffery W. Kelly[a,1], and Martin Gruebele[b,c,d,1]

Edited by Ulyana Shimanovich, Department of Materials and Interfaces, Weizmann Institute of Science, Rehovot, Israel; received October 12, 2023; accepted February 15, 2024 by Editorial Board Member Ulrich Hartl

Kinetic stability is thought to be an attribute of proteins that require a long lifetime, such as the transporter of thyroxine and holo retinol-binding protein or transthyretin (TTR) functioning in the bloodstream, cerebrospinal fluid, and vitreous humor. TTR evolved from ancestral enzymes known as TTR-related proteins (TRPs). Here, we develop a rate-expansion approach that allows unfolding rates to be measured directly at low denaturant concentration, revealing that kinetic stability exists in the *Escherichia coli* TRP (EcTRP), even though the enzyme structure is more energetically frustrated and has a more mutation-sensitive folding mechanism than human TTR. Thus, the ancient tetrameric enzyme may already have been poised to mutate into a kinetically stable human transporter. An extensive mutational study that exchanges residues at key sites within the TTR and EcTRP dimer–dimer interface shows that tyrosine 111, replaced by a threonine in TTR, is the gatekeeper of frustration in EcTRP because it is critical for function. Frustration, virtually absent in TTR, occurs at multiple sites in EcTRP and even cooperatively for certain pairs of mutations. We present evidence that evolution at the C terminus of TTR was a compensatory event to maintain the preexisting kinetic stability while reducing frustration and sensitivity to mutation. We propose an "overcompensation" pathway from EcTRPs to functional hybrids to modern TTRs that is consistent with the biophysics discussed here. An alternative plausible pathway is also presented.

HIUase | energetic frustration | unfolding mechanism | dodine | surfactant trapping

Significance

Proteins can evolve from precursors with a completely different function. This appears to be the case for human transthyretin (TTR), a tetrameric protein that carries hormones in the bloodstream and needs to be kinetically stable to avoid amyloidogenesis. We find that the bacterial enzymes from which TTR evolved are already kinetically stable. At the same time, TTR was able to lose the energetic frustration at the catalytic interface of its enzyme ancestor. Loss of frustration coupled with a change of function can be a powerful evolution strategy to afford long-lived proteins that can delay amyloid formation unless a destabilizing mutation occurs.

Members of the large family of transthyretin-related proteins (TRPs) exist in all kingdoms of life (1). Structural studies show that TRPs fold into the same tetrameric structure as transthyretin (TTR), which transports thyroxine (T4) and holo retinol-binding protein in the bloodstream, cerebrospinal fluid, and the vitreous humor (2). TRPs exhibit enzymatic activity; specifically, they play a role in purine metabolism as 5-hydroxyisourate (5-HIU) hydrolases (3). Humans, as well as certain primates, birds, and reptiles, lost 5-HIUase activity during evolution (4).

TTR is thought to have evolved from a prokaryotic 5-HIU precursor gene by a gene duplication event occurring more than 530 Mya (5, 6). Because of its relevance in human health, great effort has been made to better understand human TTR (hTTR) folding and aggregation, as well as inhibition of the latter process by small-molecule drugs (7–9). TTR is a kinetically stable protein; thus, slow tetramer dissociation into monomeric subunits that are prone to misfold and aggregate is believed to be rate limiting for protein aggregation in vitro and in vivo (10–13).

TTR and its evolutionary precursors, the TRPs, have nearly identical structures despite their low to moderate sequence conservation (30 to 50%), making TRPs and TTRs interesting model systems for quantitative biophysical studies (4). The folding biophysics of TTR is understood in some detail (14, 15), but comparatively little is known about the biophysical properties of today's TRPs that have evolved from ancestral enzymes.

The best-characterized TRP is from *Escherichia coli* (referred to as EcTRP hereafter) (1). Thermal denaturation experiments revealed that EcTRP is substantially less stable toward heat-induced denaturation than hTTR, which was attributed to a lower buried surface area and a reduced number of salt bridges and hydrogen bonds that stabilize the tetramer's interfaces (16). Prolonged incubation of EcTRP (3 d, 25 °C, pH 5.8) under mechanical stirring induces the formation of fibrillar, cytotoxic aggregates (17), but there is no evidence for aggregation of EcTRP at pH 4.0 without stirring, whereas hTTR forms amorphous aggregates in vitro under these conditions (10, 16).

By combining quantitative surfactant trapping, real-time subunit exchange, and unfolding in chaotrope solutions, we obtain an expanded view of the unfolding energy landscape of EcTRP. We demonstrate that EcTRP is as kinetically stable as hTTR under native

Author affiliations: [a]Department of Chemistry, Scripps Research, La Jolla, CA 92037; [b]Department of Chemistry, University of Illinois, Urbana, IL 61801; [c]Department of Physics, University of Illinois, Urbana, IL 61801; and [d]Center for Biophysics and Quantitative Biology, University of Illinois, Urbana, IL 61801

Author contributions: M.J. designed research; M.J. performed research; M.J. and M.G. analyzed data; J.W.K. coordinated the project; and M.J., J.W.K., and M.G. wrote the paper.

The authors declare no competing interest.

This article is a PNAS Direct Submission. U.S. is a guest editor invited by the Editorial Board.

[1]To whom correspondence may be addressed. Email: mjaeger@scripps.edu, jkelly@scripps.edu, or mgruebel@illinois.edu.

This article contains supporting information online at https://www.pnas.org/lookup/suppl/doi:10.1073/pnas.2315007121/-/DCSupplemental.

Published August 12, 2024.

conditions. Thus, the kinetic stability we see in hTTR is not a gain-of-function property acquired during TTR evolution from TRPs. Instead, it is an intrinsic property of the ancient tetrameric fold already adopted by members of the TRP family. Notably, TTR's new binding functions evolved with some loss of energetic frustration as the enzymatically active dimer–dimer interface of the TRP tetramer became a binding interface instead. Here, energetic frustration refers to nonoptimal folding free energies resulting from functional constraints (18, 19).

Despite the conservation of kinetic stability, the unfolding mechanisms of hTTR and EcTTR differ. Unfolding of hTTR is rate limited by an unusually compact, early transition state and responds to perturbation by mutation with reduced kinetic stability but without changing the unfolding mechanism, a sign of low frustration. EcTRP, on the other hand, is rate limited by a more unstructured transition state with one or more intermediates whose relative kinetic stabilities can be tuned in either direction by mutation, a sign of frustration.

Results

EcTRP and hTTR Structure and Sequence. Members of TRPs and TTR families adopt very similar three-dimensional structures (2). Superposition of the C_α atoms of a subunit of the EcTRP tetramer with a subunit from hTTR reveals high structural similarity in the eight antiparallel β-strands of the subunit's β-barrel fold (2), with some structural variation in the solvent-exposed loop regions and the domains C terminus (Fig. 1*A*). Two subunits assemble into a dimer (Fig. 1 *A*, *Middle*), which is stabilized by backbone H bonding between β-strands H and H′ from each subunit. Two dimer units interact face to face to form the tetramer, creating a dimer–dimer interface (Fig. 1 *A*, *Right*; the reader is looking into the thyroxine-binding sites between the green and red dimers). The dimer–dimer interface differs in both local structure, polarity, and sequence composition between TRPs and TTRs. In EcTRP, the dimer–dimer interface constitutes the enzyme's active site, while in hTTR, it forms the binding site for T3 and T4 hormones.

Despite very similar structures, EcTRP exhibits only 30% sequence identity to hTTR and thereby lies at the lower end of sequence identity in the TRP family (as some TRP members exhibit up to 50% sequence identity to hTTR) (Fig. 1*B*). Residues that either contribute to enzymatic activity or ligand binding are highly conserved in each protein family, but their patterns bear no resemblance to each other. All catalytic residues in TRPs were replaced by residues that contribute to T4 binding in hTTR during the course of evolution.

Nine residues (e.g., L11, F80, and L102 in EcTRP and the analogous L17, F87, and L110 in hTTR) are highly conserved in both protein families and are likely essential for protein stability and folding efficiency. We will make use of the fact that these residues are invariant, but not selected for function, as their mutation provides insights into both folding energetics and unfolding mechanisms and how these residues differ between the two protein families.

EcTRP Is a Kinetically Stable Tetramer. For proteins with quaternary structures like EcTRP and hTTR, the subunit exchange rate provides quantitative information about relevant tetramer dissociation rates under native conditions (20). For hTTR, the rate of subunit exchange agrees with the estimated rate of unfolding of the tetramer in aqueous buffer, inferred from chemical denaturation in chaotrope solutions where a linear rate extrapolation to conditions with no denaturant is employed (13, 21, 22). The agreement in rates from two seemingly unrelated experiments stems from the fact that slow tetramer dissociation is

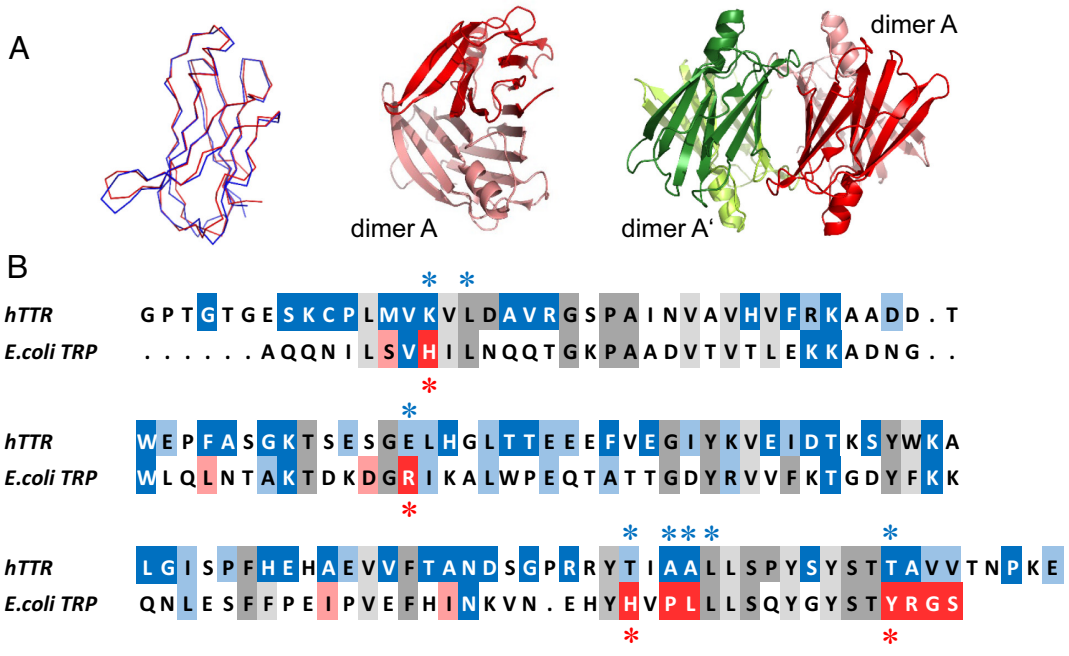

Fig. 1. EcTRP and hTTR structure and sequence. (*A*) *Left:* Backbone Cα structure of the EcTRP subunit (red), overlaid with the backbone Cα structure of the hTTR subunit (blue). *Middle:* Cartoon plot of the EcTRP dimer unit, formed by two monomeric subunits, and stabilized by a monomer–monomer interface. *Right:* Cartoon plot of the EcTRP tetramer, depicting the face-to-face interaction of two dimer units that creates a dimer–dimer interface. (*B*) Sequence of hTTR and EcTRP. Residues that form the active site of the EcTRP hydrolase and that are absolutely conserved in the TRP family are color-coded deep red. Residues with >80% sequence similarity in TRPs are color-coded light red. Residues with >80% sequence identity and similarity in TTRs are color-coded deep blue and light blue, respectively. Residues with >80% sequence identity in both TRPs and TTRs are color-coded deep gray, while residues with >80% sequence similarity in both families are color-coded light gray.

rate limiting for both subunit exchange and millisecond unfolding of released subunits in denaturant.

Subunit exchange of EcTRP was measured using an optical assay that exploits Förster resonance energy transfer (FRET). FRET donor-labeled EcTRP tetramers were mixed with FRET acceptor-labeled EcTRP tetramers. When these tetramers dissociate into donor (D) and acceptor (A) labeled subunits and reassociate back into heterotetramers, FRET between individual donor and acceptor subunits occurs (20). Specifically, a cysteine residue was engineered into a surface-exposed loop region in the EcTRP subunit for labeling with a fluorophore. The location of the cysteine in the tetramer was chosen such that the distance between a fluorophore in one subunit and a fluorophore in each of the three neighboring subunits falls within the Förster distance of the dye pair (*SI Appendix*, Fig. S1*A*). Therefore, all possible binominal combinations of heterotetramers that can be formed from the process of subunit exchange upon mixing D-labeled tetramer with A-labeled tetramer should be detectable (Fig. 2*A*).

For the dye pair used (DyLight 550/Alexa 647), there is negligible direct excitation of the A-fluorophore upon D-excitation at 535 nm (*SI Appendix*, Fig. S1*B*). Upon D-excitation, an A-labeled subunit in the EcTRP tetramer will thus only fluoresce if a D-labeled subunit is within the Förster distance ($R_0 \approx 60$ Å) of the dye pair, i.e., within the same tetramer.

When D- and A-labeled EcTRP tetramers are mixed, we initially observe high D-fluorescence (emission wavelength at 570 nm) and negligible sensitized A-fluorescence (emission wavelength at 670 nm, excitation indirectly via FRET from excited donor) (*SI Appendix*, Fig. S1*C*). Upon subunit exchange, heterotetramers with both D- and A-labeled subunits will form (Fig. 2*A*). This process can be monitored by the decrease in D-fluorescence or by the increase in A-fluorescence from intersubunit FRET (Fig. 2*B* and *SI Appendix*, Fig. S1*C*). Rate constants from single-exponential fits to the donor and acceptor fluorescence trajectories were comparable and independent of concentration (Fig. 2*C*). The measured rate constant by subunit exchange thus represents the microscopic rate constants for tetramer dissociation. The half-life of subunit exchange under native conditions (>30 h) suggests that EcTRP is a kinetically stable tetramer.

We find that the log of the subunit exchange rate constant increases linearly with denaturant up to at least 2 M urea (Fig. 2*D*), i.e., conditions where the tetramer remains folded (*SI Appendix*, Fig. S2), suggesting that urea stabilizes the transition state for tetramer dissociation upon binding.

A Rate-Expanded View of the EcTRP Unfolding Energy Landscape. We need to compare EcTRP and hTTR unfolding under native-like conditions to obtain an expanded view of their energy landscapes. Surfactants, which denature proteins at millimolar concentrations, are our tool for this purpose. Sodium dodecyl sulfate has been used to identify kinetically stable proteins in vitro and in the *E. coli* proteome (11, 12, 23). This method is useful when surfactant trapping of the denatured state is fast relative to protein dissociation or unfolding and refolding or reassociation, and irreversible, which is often the case for kinetically stable proteins. Thus, surfactant-induced denaturation should be rate controlled by protein dissociation or unfolding, and provide the microscopic rate constant of protein dissociation or unfolding, depending on which is rate limiting (24). We used surfactant trapping to benchmark EcTRP subunit exchange rates.

Dodine, a surfactant with a charged guanidine head group and a dodecyl tail, can unfold proteins below its critical micelle

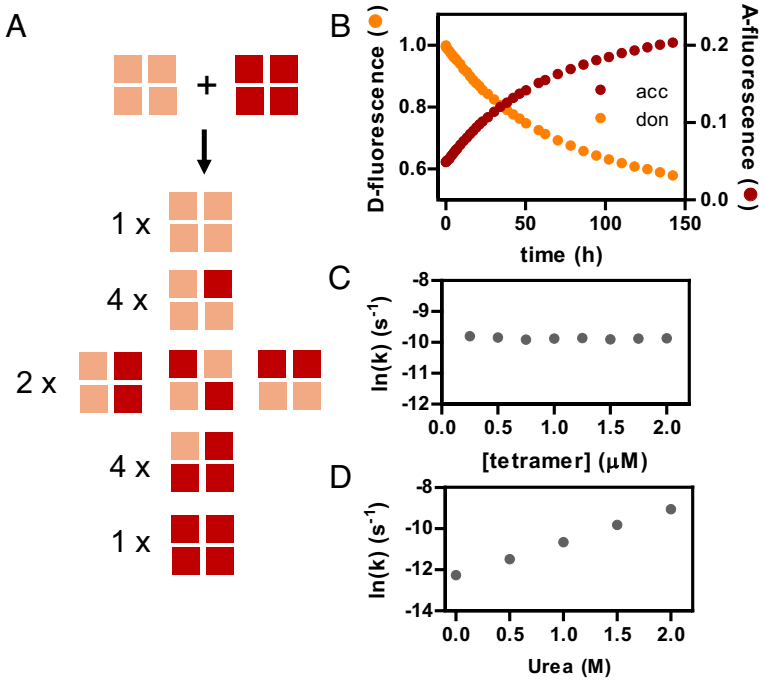

Fig. 2. Probing the kinetic stability of EcTRP by FRET-subunit exchange. (*A*) Cartoon highlighting the idea behind our FRET-based subunit exchange. The subunit exchange experiment is initiated by mixing stoichiometric amounts of donor-labeled tetramer with acceptor-labeled tetramer. Tetramers will constantly dissociate into subunits, which reassociate back into tetramers. At equilibrium, a binominal distribution of heterotetramers is formed, that contain donor- and acceptor-labeled subunits at different stoichiometric ratios. It is the time-dependent buildup of these heterotetramers that we monitor by intersubunit FRET and that provides information about tetramer dissociation dynamics under native conditions. (*B*) Donor and acceptor fluorescence emission trajectories upon mixing stoichiometric amounts of donor- and acceptor-labeled tetramer. (*C*) Dependence of the log of the subunit exchange rate constant *k* on total protein concentrations (in μM of tetramer), measured in the presence of 1.5 M urea. (*D*) Dependence of the log of the subunit exchange rate constant k on urea concentration under conditions where the tetramer remains predominantly folded.

concentration (CMC ≈ 4 mM) and at ambient temperature (25, 26). In low salt buffer to prevent dodine aggregation (10 mM Hepes, pH 7.5), dodine unfolds EcTRP cooperatively with a transition midpoint of 0.7 mM dodine (Fig. 3*A*) at a protein concentration of 1.5 μM tetramer. The transition is complete below the CMC of dodine in the buffer used, and no further protein unfolding is observed under conditions where micelles form. Tryptophan fluorescence and far- and near-UV circular dichroism (CD) reveal that dodine-denatured EcTRP is non-native but retains residual secondary and tertiary structure (*SI Appendix*, Fig. S3). Whether the residual structure is induced by binding of dodine to the unfolded protein (27, 28) cannot be decided by these experiments alone.

At concentrations where dodine-induced equilibrium unfolding reaches the posttransition plateau, dodine denatures EcTRP with single exponential kinetics (*SI Appendix*, Fig. S4). Dodine also accelerates EcTRP unfolding in urea solutions (e.g., 5 M urea) (Fig. 3*B*). In either case, the log of the unfolding rate increases linearly to a dodine concentration of at least 3 mM, i.e., below the CMC of dodine (Fig. 3*B*). The slope of the rate plot is smaller in urea than in aqueous buffer, suggesting that dodine binds to the transition state for unfolding with high affinity, but becomes outcompeted by urea when the latter is present at molar excess. The ability to estimate dodine-corrected unfolding rates in aqueous solutions and in solutions with denaturant by linear extrapolation gives us access to a rate-expanded view of the energy landscape of unfolding that covers the entire experimentally accessible denaturant concentration range (0 to 10 M urea) (Fig. 3*C*).

The rates well above the midpoint of equilibrium unfolding of EcTRP were measured directly in urea, and therefore no rate extrapolation is necessary (*SI Appendix*, Fig. S5). The rates below the midpoint of urea unfolding are inaccessible to conventional kinetic unfolding experiments due to the dominance of the folding rate and were obtained from linear extrapolation in dodine/urea solutions (Fig. 3*C* and *SI Appendix*, Fig. S6). We observe no significant offset or discontinuity in the two datasets. Under native-like conditions, the log of the rates of unfolding measured by dodine trapping reproduces the linear trend seen with subunit exchange (*SI Appendix*, Fig. S7), suggesting that both techniques monitor the same rate-limiting tetramer dissociation step. We attribute the slightly lower rates measured by subunit exchange to protein labeling with bulky fluorophores and the engineering of a cysteine for fluorophore labeling. Thus, expanding the window into unfolding to include slow unfolding rates may be more accurate with dodine, which does not require protein modification.

At higher denaturant concentrations, the plot of the log of the unfolding rate of EcTRP deviates from linearity (*SI Appendix*, Fig. S7). The pronounced downward curvature in the log of the rate constant of EcTRP resembles that reported for GFP, another kinetically stable protein. In GFP, there was additional spectroscopic evidence for transient, stable unfolding intermediates that become rate limiting for unfolding at high denaturant concentrations (29). We postulate that similar kinetic traps are populated upon unfolding of EcTRP. The conformational intermediates in EcTRP must be formed in the context of intact tetramers because subunit exchange occurs at a much slower rate than observed here, with single exponential kinetics, and without a significant burst subunit exchange phase even when using manual mixing. The relative free energy of the intermediates or traps is also sensitive to denaturant and mutational perturbation (vide infra), which is a signature of energetic frustration in EcTRP.

Compared to EcTRP, hTTR exhibits much higher kinetic resistance to chemical denaturation (Fig. 3*D*), as manifested by a low slope in the "Chevron plot" (the log of unfolding rate vs. denaturant concentration), despite very similar apparent thermodynamic stabilities (*SI Appendix*, Fig. S2) at zero denaturant. The log of the unfolding rate of hTTR also varies very little, and approximately linearly, with denaturant concentration. As the

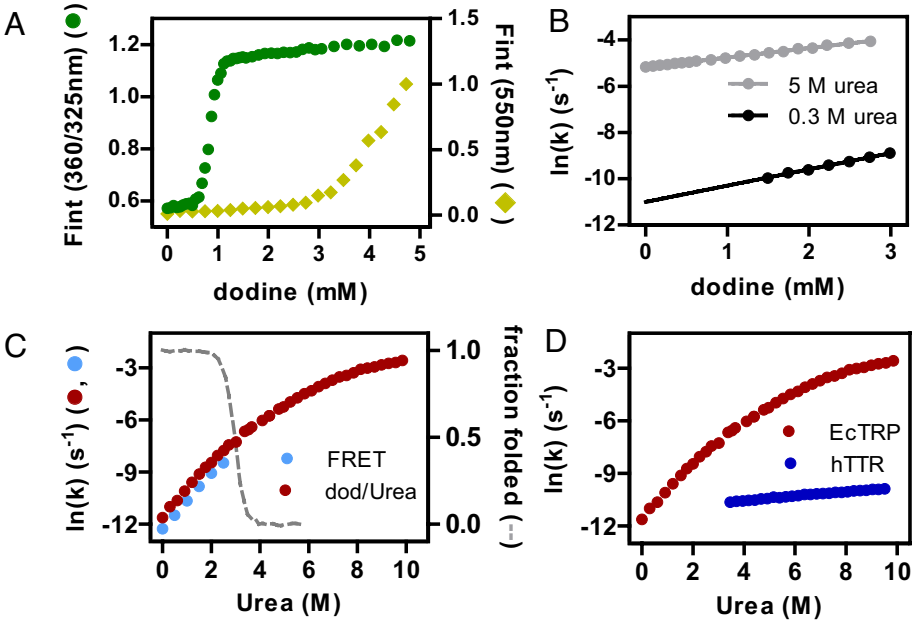

Fig. 3. Dodine rate expansion and a full view of the energy landscape of EcTRP unfolding. (*A*) Dodine cooperatively denatures the EcTRP tetramer at millimolar concentrations and below the onset of dodine micelle formation (25 °C, 72 h incubation). (*B*) Dodine unfolds EcTRP with single exponential kinetics. The log of the rate constant *k* for unfolding increases linearly with dodine concentration, affording linear rate extrapolation to obtain dodine-corrected unfolding rate constants. (*C*) Under conditions where the tetramer is stable, the log of the unfolding rate constant and the log of the subunit exchange rate increase similarly, and linearly with urea concentration. At high urea concentration, the rate plot deviates from linearity, suggesting the presence of transient unfolding intermediates or kinetic traps that become rate limiting for unfolding. (*D*) The rate plot of hTTR differs significantly from the rate plot of EcTRP, and is consistent with simple two-state unfolding of a minimally frustrated protein. Despite obvious differences in unfolding mechanism, the extrapolated rates indicate that both proteins exhibit similar kinetic stabilities under native conditions.

slope of the kinetic unfolding arm is a measure of the change in solvent accessible surface area (SASA) between the intact tetramer and the transition state barrier, the kinetics of hTTR is in excellent agreement with apparent two-state unfolding via a single transition state barrier with near-native solvent exposure.

The dimer–dimer interface of hTTR is optimized for T4 binding, and in apo-TTR, partially filled with structural water (30). Dimer–dimer contacts in hTTR are made by the interaction of two loop structures connecting β-strands A and B and G and H in each subunit (30). Protein engineering (31) and more recent molecular dynamics simulations (32) suggest that hTTR tetramer dissociation is rate limited in part by a hydration barrier and tetramer dissection along the dimer–dimer axis into two transient, unstable dimers. The small change in SASA upon tetramer dissociation into folded dimers that this model predicts is consistent with the shallow slope of the experimental rate plot of hTTR.

Despite obvious mechanistic differences in unfolding between hTTR and EcTRP, extrapolation of the unfolding rates of hTTR suggests that under native conditions, both proteins show very similar rates of tetramer dissociation. A direct verification of this hypothesis, however, was not possible due to binding of dodine to the intact hTTR tetramer (vide infra) and sigmoidal exchange kinetics, suggesting nontrivial interactions of attached fluorophores with the hTTR tetramer. The high kinetic stability of hTTR is therefore not the consequence of its evolution from an unstable, ancient enzyme, but due to the high intrinsic kinetic stability of the tetramer fold that both the TRP and TTR protein families adopt. In that sense, the enzyme was poised for mutation of its active site into a kinetically stable blood plasma carrier protein.

Contrasting Structural Properties of the EcTRP and hTTR Dimer–Dimer Interface. Having demonstrated both conserved kinetic stability and a lack of conserved unfolding mechanism during evolution of hTTR and EcTRP, we next pursued a mutational approach to better understand, at a molecular level, what causes the two structurally very similar proteins to unfold along mechanistically different pathways. For the design of suitable mutants, we focus first on the dimer–dimer interface, where the two proteins differ the most (*SI Appendix*, Fig. S8) (3). In EcTRP, the presence of the bulky Y111 residue located in β-strand H and nested deep inside the dimer–dimer interface sterically blocks access of T4 hormone ligand to this interface. The Y111 sidechains from one subunit and from the juxtaposed subunit across the dimer–dimer interface stabilize each other by side-chain hydrogen bonding. The sidechain of Tyr111 further engages in hydrophobic interaction with leucines L11 and L102, as well as interacting with Q13 from the same juxtaposed subunit. Being highly conserved among TRPs and TTRs, analogous leucine residues are present in hTTR: L17 and L110.

The side-chain conformation of hTTR L17 and L110 and their interactions change significantly relative to EcTRP because the bulky Tyr is replaced by a smaller threonine residue (T119) to open the interior of the cavity and hence to accommodate the T4 hormone ligand. L110 can still make a hydrophobic contact with T119, but its side chain faces away from the T4 ligand, while it faces toward the ligand in EcTRP. The L11–Y111 interaction in EcTRP is lost in hTTR but is compensated for by a side-chain interaction with a conserved V121 residue in the C-terminal extension of hTTR. Residues A120-T123 in this C-terminal extension elongate β-strand H and allow the formation of two stabilizing backbone H bonds with β-strand G of the same subunit. In stark contrast, in EcTRP the extreme C terminus (residues R112-G113-S114) folds back toward the dimer–dimer interface. The resulting loss of the two backbone H bonds with β-strand G in EcTRP is compensated for by the absolutely conserved residue R112 in EcTRP, whose side-chain conformation mimics the C-terminal extension in hTTR and enables the formation of two equivalent side-chain-to-backbone H bonds with β-strand G (2). Arg112 is also a key residue in mediating side-chain contacts with another subunit across the monomer–monomer interface because its long side-chain stem constitutes part of the hydrophobic lining to accommodate the phenyl ring of residue F80 that protrudes from another monomer across the monomer–monomer interface (*SI Appendix*, Fig. S9).

Finally, residue Q13 in EcTRP is replaced by Ala in hTTR. In *Xenopus* TRP, this residue is an Isoleucine. Cendron et al. (3) showed that for conversion of *Xenopus* TRP into a T4-hormone binder with no significant HIUase activity, two mutations are sufficient—Y116T (Y111T and Y119T in EcTRP and hTTR, respectively) and I16A (Q13A in EcTRP). Note that the consensus residues at position 13 in HIUases are threonine and valine. The Y116T mutation alone is not sufficient for TTR-like binding affinity, presumably because the I16A changes the orientation of bulky side chain L107 (L102 in EcTRP) in such a way that it resembles the orientation of L110 in hTTR (3).

Frustration of the EcTRP but Not the hTTR Tetramer Interfaces. Using these structural considerations, we were able to design targeted mutations that perturb selective interactions in the dimer–dimer and monomer–monomer interfaces in either protein context to address how the mechanistic differences in unfolding between hTTR and EcTRP result from changes in tetramer interface energetics and cooperativity. Side-chain truncation to alanine, either individually (e.g., at L11A, L102A, R112A) or pairwise (at L11A/L102A in EcTRP) perturbs existing interactions without introducing new ones, while Y111 in EcTRP was mutated to Thr, the natural residue in hTTR.

For hTTR, all variants exhibit lower thermodynamic stability (*SI Appendix*, Fig. S10) and reduced kinetic stability (Fig. 4). This is the expected result for a circulating hormone carrier protein with low frustration and optimized for kinetic stability in a harsh biological environment: It will be hard to find mutations that actually further stabilize, or kinetically stabilize, such a protein.

The Y111T mutation in EcTRP destabilizes the tetramer thermodynamically and accelerates tetramer unfolding (Fig. 4 and *SI Appendix*, Fig. S10). The overall shape of the rate plot does not change, except above 8.5 M urea, where the extreme rollover seen in the wild type is no longer visible. In contrast to the EcTRP wild type, we found that EcTRP Y111T is not amenable to rate expansion by dodine trapping, presumably because the alkyl tail of dodine inserts into the opened dimer–dimer interface and stabilizes the tetramer (*SI Appendix*, Fig. S11), in analogy to how medium-length alkyl chains bind to the hTTR dimer–dimer interface (33). Subunit exchange, shown above to yield similar results as dodine expansion, was therefore used to fill in the rates at conditions where the tetramer is folded. This leaves a window of denaturant concentration that coincides with the equilibrium unfolding transition of Y111T, where no rates can be reported by unfolding in denaturant only. All EcTRP mutants that carry the Y111T show this behavior. All other variants that contain Y111, including variants L11A and L102A that have the same side-chain contacts truncated as Y111T, do not show this effect, and are amenable for rate expansion as described for the EcTRP wild type in *SI Appendix*, Fig. S11.

EcTRP variants L11A, L102A, and L11A/L102A that reciprocally perturb the same hydrophobic contacts with Y111 are kinetically more stable than the EcTRP wild type (Fig. 4). L11A also

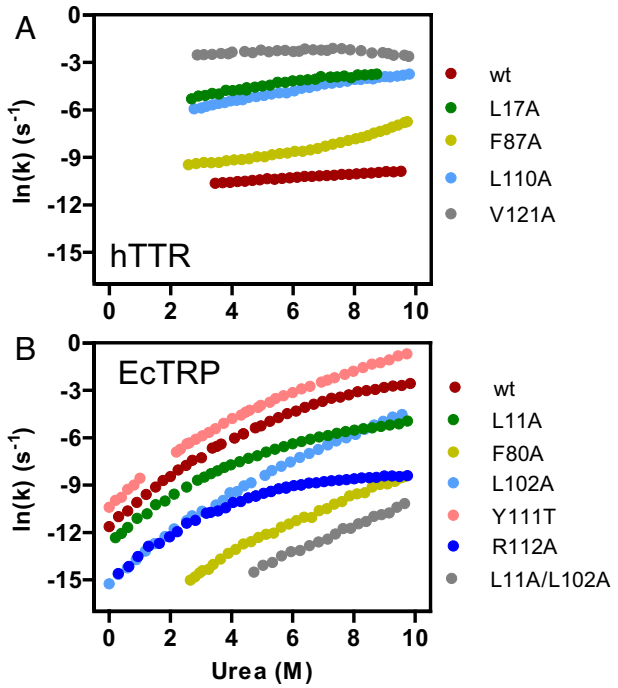

Fig. 4. Kinetic analysis of (*A*) hTTR and (*B*) EcTRP variants that carry mutations to selectively perturb conserved hydrophobic contacts at the dimer–dimer and monomer–monomer interfaces of each tetramer. EcTRP variants with very high kinetic stability were not rate expanded. TTR wild type and variants were also not rate expanded, as dodine binds to the less constricted dimer–dimer interface in hTTR and stabilizes the tetramer against unfolding in urea. For details, see the main text.

increases the kinetic rate rollover at high denaturant, while L102A renders the rate plot more linear. The kinetic stability of L11A/L102A, which ranks highest in the number of perturbed native contacts, is highest and exceeds the sum of the individual mutants, especially under more stabilizing conditions. This observation marks a particularly clear example of frustration, which makes it easier to find stabilizing residues by mutating EcTRP, and even cooperatively stabilizing residues in EcTRP than in hTTR. Reinforcing this picture, the unfolding kinetics of R112A follows the trend seen in L11A, i.e., this mutant also is kinetically more stable than the EcTRP wild type (especially under conditions of high denaturant stress, see Fig. 4 and *SI Appendix*, Fig. S12).

Increased kinetic stability is also observed with the F80A variant that eliminates the contact of the F80 sidechain with R112, a contact that is absolutely conserved in the TRP family. Like L11A/L102A, F80A should destabilize the protein, but in analogy to L11A/L102A, we find that the F80A/R112A double mutation increases EcTRP kinetic stability even more than F80A alone, and to a level that EcTRP resists any significant unfolding in 10 M urea over a period of 3 mo (*SI Appendix*, Fig. S10*C*). The analogous mutation in hTTR (F87A) is destabilizing. Mutants F80A and R112A are additional examples that unveil frustration in EcTRP. Because the conserved C terminus in EcTRP plays a structural role in stabilizing the active site, R112 is the only residue that can simultaneously provide the supporting hydrophobic interaction with F80 from a subunit across the monomer–monomer interface and stabilize the subunit it resides in through H bonds with strand G. Such a "servant to two masters" role may off-balance tetramer energetics globally. Equally possible is that R112, which immediately follows Y111 in sequence, just transmits frustration originating in the dimer–dimer interface to the monomer–monomer interface, and through its side-chain contact with F80.

In hTTR, Ala120 replaces R112 in EcTRP, and a larger number of residues from one subunit contribute to binding of the phenylalanine side chain from the other subunit (30), which may make this interaction stronger and energetically optimized in hTTR, but also more vulnerable to perturbation by mutation (Fig. 4 and *SI Appendix*, Fig. S9).

Frustration, as seen upon mutagenesis at many sites in EcTRP, is not detectable in hTTR, which could be the result of functional evolutionary constraints and the particular way the monomer–monomer and dimer–dimer interfaces in the EcTRP have to cooperate structurally and energetically to assure biologically relevant HIUase activity.

Tyr111 Is the Master Residue for Frustration in EcTRP. Having demonstrated frustration in EcTRP at multiple sites, but an absence of frustration in hTTR, we wondered whether frustration in EcTRP would persist upon mutation of Tyr111 to Thr, the residue found in hTTR. We found that in the Y111T background, L11A and L102A become "normally" behaving, kinetically destabilizing variants, with unfolding rates similar to the L17A and L102A variants in hTTR (*SI Appendix*, Fig. S13). The pronounced curvature of R112A is reduced, although R112A remains a kinetically stabilizing mutation in the Y111T context. Only F80A/Y111T deviates from this trend in that it shows slightly enhanced kinetic stability at high denaturant, and a slight increase in the curvature in the unfolding rate plot at high chaotrope stress.

The observation that Y111 in EcTRP determines whether mutational truncation of a contacting sidechain from a neighboring residue is kinetically stabilizing (Y111 background) or destabilizing (T111 background) is interesting on its own. It demonstrates that Tyr111 is the master residue for energetic frustration in EcTRP among all the mutations we tested. As Y111 is also a key residue for function, frustration in EcTRP seems to be the consequence of 5-HIUase functional evolutionary constraints. No such catalytic constraints exist in hTTR, other than that it must be flexible/rigid enough to bind T3 and T4 hormones with biologically relevant affinity over the biologically relevant time scale than hTTR circulates in plasma (2 to 3 d). It is plausible that such function as a passive hormone carrier could have evolved while monomer–monomer and dimer–dimer interfaces remained energetically optimized.

How TRP Frustration Changed during Evolution into TTRs. The absorbance spectrum of the nonfluorescent T4-hormone overlaps with the emission spectrum of TTR Trp fluorescence. Thus, T4-binding-associated TTR fluorescence quenching can be exploited to probe T4 binding to hTTR and EcTRP–hTTR hybrids. Cendron et al. used T4-binding-induced fluorescence quenching to demonstrate that in *Xenopus* TRP, two amino acid substitutions (Y116T/I16A) are sufficient to install hTTR-like T4 binding with simultaneous loss of HIUase activity (3). Either mutation alone does not elicit this effect, demonstrating that, at least in *Xenopus* TRP, residues I16 and Y116 must have evolved prior to formation of the full hTTR T4-binding interface.

The corresponding mutations in EcTRP are Q13A and Y111T (Fig. 5*A*). Unlike *Xenopus* TRP, however, the fluorescence of EcTRP is already significantly quenched in the native tetramer, and addition of T4 to the protein solution resulted in slight scattering, complicating the interpretation of T4-binding data. Small-molecule binding in hTTR and EcTRP–hTTR hybrids was therefore probed using a recently developed covalent modification assay. Fluorogenic small-molecule ***A2*** is a stilbene that binds selectively to hTTR and remains nonfluorescent until it's thioester functional group undergoes a

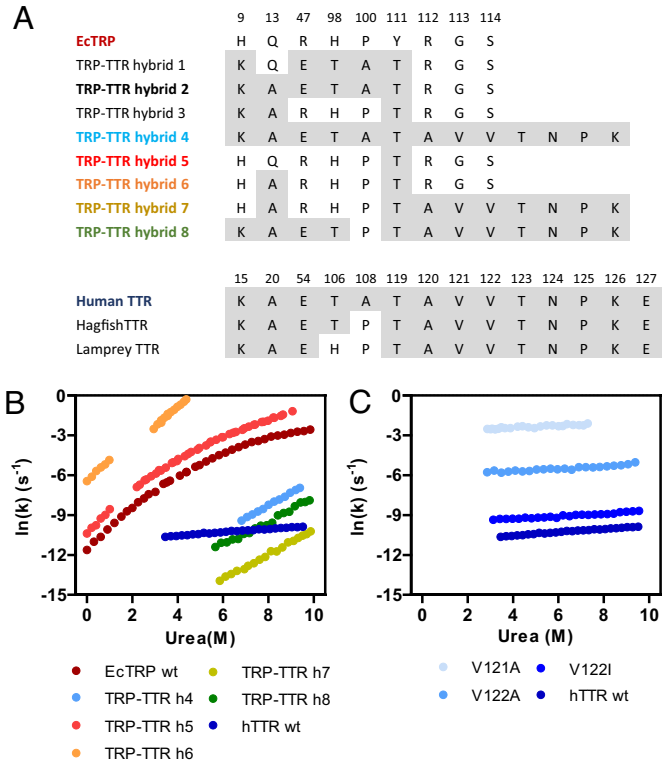

Fig. 5. Frustration in EcTRP and hTTR from an evolutionary perspective. (*A*) Sequence of EcTRP and hTTR highlighting the residues in the dimer–dimer interface and the C terminus that changed during evolution of hTTR from ancient TRPs. TRP–TTR hybrids 2 and 4 to 8 are hypothetical evolutionary intermediates (see the main text for details). (*B*) Unfolding kinetics of EcTRP, hTTR, and TRP–TTR hybrids. (*C*) Unfolding kinetics of the hTTR wild type and disease-associated variants in the C-terminal extension.

chemoselective reaction with the pKa-perturbed ε-amino group of Lys15 to create a bright blue fluorescent conjugate (*SI Appendix*, Fig. S14 *A*, *Top*). Previous work demonstrates that ***A2*** activation is highly specific for hTTR and strictly depends on the presence of the pKa-perturbed Lys15 in the T4-binding interface. As ***A2*** is comparable in size to T4, and structurally complements the T4-binding interface of hTTR (*SI Appendix*, Fig. S14 *A*, *Bottom*), we can use ***A2*** binding-induced conjugation as a proxy for T4 binding in EcTRP and EcTRP–hTTR hybrids thereof.

Reacting hTTR (2 μM tetramer) with a 10-fold excess of ***A2*** stilbene (20 μM) affords the ***A2***-based fluorescent conjugate on the minute time scale (*SI Appendix*, Fig. S14*B*). However, no ***A2***-based conjugate formation is detectable with **EcTRP–hTTR hybrid 1**, which carries the K9K/R47E/H98T/P100A/Y111T mutations (Fig. 5*A*), and thus has the fully reconstituted T4-binding site of hTTR (*SI Appendix*, Fig. S14*C* and Fig. 5*A*). Introducing the Q13A mutation in EcTRP–hTTR hybrid 1 to create **EcTRP–hTTR hybrid 2** (Fig. 5*A*) allows ***A2*** binding and hybrid 2 conjugate formation (*SI Appendix*, Fig. S14*C*), presumably because Q13A further sterically unblocks the dimer–dimer interface. From a functional perspective, it is thus unlikely that EcTRP–hTTR hybrid 1 is a biologically relevant intermediate, as the T4-binding site would have to evolve without the selection benefits of ligand binding.

Despite binding and conjugate formation with the ***A2*** ligand, the kinetics of the ***A2*** reaction with EcTRP–hTTR hybrid 2 is significantly slower than by hTTR. Even slower ***A2*** conjugation is detectable with **EcTRP–hTTR hybrid 3** (*SI Appendix*, Fig. S14*C*), which carries the interface-opening mutations Q13A/Y111T and the Lys (H9K) required for ***A2*** activation, but retains EcTRP wild-type residues at position 47, 98 and 100.

With **EcTRP–hTTR hybrid 4**, which carries the C-terminal extension in addition to the full T4-binding site from hTTR, we observe the ***A2*** binding/conjugation obtained with hTTR, but at a slowed rate (*SI Appendix*, Fig. S14*E*). The C terminus, although not directly contributing to ***A2*** conjugation or T4 binding in hTTR, is nevertheless important for fine-tuning ligand-binding activity and, like P100A, drastically increases tetramer stability in urea equilibrium unfolding experiments (*SI Appendix*, Fig. S15).

Having demonstrated that the Q13A and Y111T mutations in EcTRP likely occurred early in the evolution of hTTR from TRP precursors, we next direct our attention to the biophysics and kinetic stability of evolutionary plausible EcTRP–hTTR hybrid variants (for sequences, see Fig. 5*A*). The unfolding rate plot of EcTRP Q13A/Y111T (**EcTRP–hTTR hybrid 6**) is linear, and lacks the curvature seen in EcTRP wt and EcTRP Y111T (**EcTRP–hTTR hybrid 5**) that we attribute to stable unfolding intermediates and frustration (Fig. 5*B*). Unlike L11A/L102A and F80A/R112A that exacerbate frustration, Q13A and Y111T are thus mutations that, when combined, reduce frustration and afford apparent two-state unfolding. The unfolding rate of EcTRP–hTTR hybrid 6 is comparable to the unfolding rate of TTR variants V122A and V122I, which cause ATTR amyloidosis in humans (Fig. 5*C*). As EcTRP itself is an amyloidogenic protein (17), we thus hypothesize that an early hybrid, such as EcTRP–hTTR hybrid 6, could have been prone to tetramer dissociation and subunit misfolding-associated aggregation when circulating in an ancient host, triggering a compensatory structural change.

Elongation of the C terminus, as seen in today's TTRs, may have been such a compensatory event. Very importantly for avoiding a kinetic stability bottleneck in TTR evolution, the exchange of the conserved TRP C terminus in EcTRP–hTTR hybrid 6 with the elongated C terminus from hTTR to create **EcTRP–hTTR hybrid 7** (Fig. 5*A*) increases kinetic stability of hybrid 6 by up to three orders of magnitude in 9 M Urea, exceeding even the already high kinetic stability of wild type hTTR (Fig. 5*B*).

From EcTRP–hTTR hybrid 7, four more amino acid substitutions are necessary to reconstitute the T4-binding site of hTTR (Fig. 5*A*). TTRs from both lamprey and hagfish still feature the conserved, but destabilizing (*SI Appendix*, Fig. S15) active-site proline in HIUases, but already have the C-terminal extension from hTTR (34). We thus argue that His9, Arg47 and His98 were replaced with Lys, Glu and Thr in early TTR-like hybrids *after* the C-terminal extension evolved (**EcTRP–hTTR hybrid 8**), but before the replacement of the interfacial proline of TRPs by an alanine in hTTR (EcTRP–hTTR hybrid 4) (Fig. 5*A*). Lysine in hTTR forms a stabilizing salt bridge with bound T4, which may have been advantageous for T4-binding affinity tuning early in vertebrate development (30). Although full development of the T4-binding site occurred at the expense of kinetic stability, the enhanced kinetic stability of a mutant such as EcTRP–hTTR hybrid 7 relative to even wild type hTTR provided the necessary overcompensation to allow the active site to evolve while avoiding adverse tetramer dissociation in transitional TTRs during evolution (Fig. 5*B*).

As a viable alternative explanation, it is also possible that the full T4-binding site and the gate opening substitution at position 13 (Q13A or I16A in *Xenopus*) developed in TRPs prior to the C-terminal extension (EcTRP–hTTR hybrid 2, Fig. 5*A*), thus bypassing hybrids 7 and 8 in our model. We believe that this scenario is less likely, given that in lamprey and hagfish TTR, the C terminus evolved prior to the full hTTR T4-binding site. We also note that the kinetic stability of hybrid 2 is comparable to

hybrid 6 under native conditions (*SI Appendix*, Fig. S16). Thus, even if TTR evolved from TRPs by first developing the full T4-binding site prior to installing the stabilizing C-terminal extension, our key proposal—that kinetic stability of TRP had first to be compromised before it could be regained fully later—still holds.

Our simple model for evolution of TTRs from TRPs considers only the changes in the dimer–dimer interface and at the C terminus, the two most obvious regions for structural changes. Yet the reconstituted ancestor of all contemporary transthyretins (*TTR ancestor* hereafter) only shows about 50% sequence identity to modern TTRs, so mutations also had to occur elsewhere in the tetramer structure (6). The exact series of events cannot be reconstituted at present. Some mutations could have brought early TRP–TTR hybrids to only borderline kinetic stability, changing the sequence of events we propose here, while other mutations may have occurred early in evolution and were essential for evolution, but were selected against at a later stage, and left no footprint in today's sequences.

Discussion

Circulating proteins, among others, have the interesting property of having kinetic stability, whereby large barriers prevent premature dissociation of a complex or unfolding of a monomeric protein (10, 12, 24). Yet it has remained difficult to study the compensation between kinetic stability and function due to a lack of techniques that can quantify dissociation under native-like conditions. TTR, whose kinetic stability is thought to be necessary for its function, is a case in point. Here, we show that a bacterial TTR enzyme with very similar quaternary structure can be equally kinetically stable, and we chart a path whereby overcompensation allowed a new binding function to evolve in TTR while maintaining sufficient kinetic stability for circulation.

Elucidating this path is made easier by supporting sequence information with biophysical unfolding and dissociation energetic information. Acquiring these data required a key method: dodine trapping, which can be a reliable kinetic approach to expand the experimentally accessible unfolding rates all the way to native conditions and to provide a direct full view of the energy landscape of unfolding. We benchmarked the data from dodine trapping with data from subunit exchange, and we found that both techniques yield comparable results. However, dodine could prove to be more reliable because it is a perturbative method (can be tuned continuously to zero concentration) that does not require protein labeling.

Whether dodine trapping and rate expansion is applicable to a larger set of proteins remains to be shown. As a limitation, we show that the structural opening of the dimer–dimer interface in the EcTRP wild type by an Y111T mutation enables dodine to bind to the tetramer and slow down its unfolding. Limitations, however, also exist for commonly used denaturants. Urea is intrinsically unstable and can modify primary amines in proteins (35). Both guanidine chloride and guanidine thiocyanate are charged and behave nonideally at the necessary high concentration. When used with TTR, they also behave as kosmo-chaotropes, as binding of the anion to the T4-binding interface stabilizes the tetramer at low to moderate denaturant concentrations (36).

We applied dodine trapping to EcTRP, a HIUase enzyme that lies at the lower end of this sequence identity spectrum and is also different from the presumed *TRP–TTR ancestor*, the last common ancestor of TRPs prior to the gene duplication event and the emergence of TTRs (6). Targeted mutations of EcTRP, such as at L11A, F80A, L102A, and R112A, reveal energetic frustration in EcTRP, for which we find no evidence in hTTR, whose constraints for T4 binding are more permissive. Indeed, there is even cooperative frustration in EcTRP. Application of the frustratometer did not differentiate hTTR and EcTRP sufficiently, which we attribute to the frustration in the dimer–dimer and monomer–monomer interfaces of kinetically stable EcTRP enzyme being mostly a transition state, effect.

With the limited sequence information available to us today, a full reconstruction of the series of events leading to modern hTTR from its enzymatic ancestors is not possible. Nonetheless, we believe the simple model discussed by way of the data in Fig. 5 captures the essence of the two main structural changes that occurred—the sculpting of an enzymatic active site into a binding cavity for thyroid hormones around Y111 and the extension of the C terminus in hTTR as a compensatory mechanism to maintain the already existing kinetic stability of the enzymatic ancestor of hTTR. Plausible hybrid sequences demonstrate that the kinetic stability of hTTR likely went through compensatory cycles. One such cycle was triggered by mutation of the bulky, conserved interface Y111 and the opening of the binding site for small-molecule ligands, which removed most of the functional constraints and frustration in the enzyme, but at the cost of newly gained kinetic instability. The likely compensatory stabilizing event was the C-terminal extension, which in hTTR does not directly contribute to function but helps avoid aggregation unless it is perturbed by disease-associated mutations (Fig. 5*C*).

Materials and Methods

Reagents. Urea (BioUltra, for molecular biology, >99%), dodine (acetate salt), and DiO (3,3′-dioctadecyloxacarbocyanine perchlorate) were obtained from Sigma. Sodium phosphate (monobasic monohydrate) and Hepes [4-(2-hydroxyethyl)-1-piperazineethanesulfonic acid, >99%] were supplied by Fisher Scientific. DyLight 550 maleimide and Alexa 647 maleimide fluorophores were obtained from ThermoFisher. All other reagents were of analytical grade. The concentration of urea solutions was determined refractometrically.

Protein Expression, Purification, and Labeling.

Protein expression. As EcTRP is an endogenous *E. coli* protein, and we intended to study variants of wild type EcTRP expressed in *E. coli*, we constructed a vector for expression EcTRP with an N-terminal penta-Histidine tag (His_5-tag) for cytoplasmic expression. It was shown before that the presence of an N-terminal His-tag does not significantly compromise protein function (37), and because no activity assays were performed in the present work, and the focus was on unfolding in surfactant and surfactant/urea solution, the His-tag was not proteolytically removed. The presence of a His_5-tag accelerates purification, improves the yield of destabilized variants, and affords the isolation of EcTRP variants away from the cell extract in less than 30 min, minimizing the risk of contamination of the overexpressed protein by subunit exchange with endogenous, wild type EcTRP.

hTTR was expressed using a previously published vector (37). Residue Cys10 was replaced by Ala to avoid oxidation and posttranslational modification, which can affect the biophysical measurements, and a His_5-tag was added to the flexible N terminus (the first nine residues of TTR are disordered and not visible in X-ray structures) to facilitate purification of disease variants. The presence of the His_5-tag in the unstructured N-terminal region does not affect the biophysical properties of hTTR (38).

Purification. His_5-tagged proteins were purified by immobilized metal affinity chromatography (IMAC) in IMAC buffer (50 mM sodium phosphate and 500 mM sodium chloride) using prepacked columns (5 mL bed volume). For a typical protein preparation, cells from 2 L Luria–Bertani culture medium were harvested by centrifugation (4,000 × g, 30 min, 4 °C) and resuspended in IMAC buffer. The lysed bacterial resuspension was transferred to 2 mL Eppendorf tubes and centrifuged (5 min, 15,000 × g, 25 °C). The supernatant was collected, filtered through a PVDF membrane, and manually passed twice through an IMAC column with a syringe. The column was then mounted on a chromatography system

(AKTA Pure, GE Healthcare) and washed with IMAC buffer (10 mL/min) until the absorbance at 280 nm of the column eluate reached baseline levels. Because our target proteins are tetramers with each subunit His_5-tagged, we found that the column-loaded tetrameric EcTRP or hTTR does not elute in IMAC buffer supplemented with 160 mM imidazole, conditions were contaminants, and misfolded monomers or dimeric assemblies of EcTRP or hTTR would elute. After the column eluate reached baseline levels, tetrameric protein was eluted in IMAC buffer, supplemented with 800 mM imidazole.

The eluted protein solution was transferred to a centrifugal concentrator (Sartorius Vivaspin, MWCO 5000) and buffer exchanged into either 10 mM Hepes, pH 7.40 (EcTRP), or 50 mM sodium phosphate, pH 7.40 (TTR), using 10 cycles of concentration and dilution in a benchtop centrifuge (3,500 rpm, 25 °C). The buffer-exchanged, concentrated protein solution (typically 5 mL) was transferred to a dialysis membrane (MWCO 5000) and dialyzed twice against 5 L of 10 mM Hepes, pH 7.40 (EcTRP) or 50 mM sodium phosphate, pH 7.40 (>6 h per dialysis cycle). Protein concentrations were determined spectrophotometrically (NanoDrop, ThermoFisher) using molar extinction coefficients calculated from the amino acid composition. Purified protein was either used immediately (TTR), or stored for a maximum of 1 wk at 4 °C.

Labeling. For measurements of tetramer subunit exchange of EcTRP, we used a single Cys variant with an N-terminal His_5-tag and an Asn94Cys mutation in a solvent-exposed loop. The variant was expressed and purified as mentioned in the previous paragraph, except that 0.5 mM DTT was included in the IMAC buffer to prevent Cys oxidation and suppress the formation of interchain cross-links during purification. Immediately after the protein was eluted from the IMAC column, the DTT concentration was increased to 2 mM. The reduced protein solution was concentrated (3 to 5 mL) in a benchtop centrifuge (3,600 rpm, 25 °C), and injected onto a preparative-scale size exclusion column (HiLoad 16/600 Superdex 75, GE Healthcare) that was equilibrated in SEC buffer (50 mM phosphate, pH 7.40, and 100 mM sodium chloride). Fractions that contained tetrameric protein were pooled and immediately reacted with a solution of DyLight 550 maleimide (for Cys labeling with a FRET donor), or Alexa 647 maleimide (for Cys labeling with a FRET acceptor). To ascertain a high degree of protein tetramer labeling, the fluorophore was added from a stock solution in water (1 mM) to give a fourfold stoichiometric excess of dye over the thiol side chains in the protein (assuming all thiols are reduced and reactive). After incubation for >4 h at 25 °C, a slurry of activated thiol resin in SEC buffer (GE Healthcare) was added to the protein solution to capture unmodified protein. The solution was centrifuged and the supernatant was manually passed through an IMAC column (1 mL bed volume) to remove unreacted dye. The IMAC resin was washed with 50 mL IMAC buffer, and fluorophore-labeled protein was eluted from the column in IMAC buffer with 800 mM imidazole. The eluted protein was buffer exchanged into 10 mM Hepes, pH 7.40, using repeated cycles of concentration and dilution in a benchtop centrifuge, followed by passage of the concentrated protein solution (300 to 500 μL) through a 5 mL PD10 column (GE Healthcare), equilibrated in 10 mM Hepes, pH 7.40. The concentration of labeled protein was determined spectrophotometrically, using published molar extinction coefficients of the fluorescent dyes. Dye labeling efficiency was estimated from absorbance measurements at the dye absorbance maximum, and measurements of protein absorbance at 280 nm, that was corrected for the contribution of the attached fluorophore. Labeling efficiencies of at least 85% were routinely obtained. No efforts were made to further purify labeled from nonlabeled protein.

Fluorescence Measurements. Fluorescence measurements were performed with a Jasco Model FP-8500 Spectrofluorometer using a 1 cm path length quartz cuvette. Protein Trp fluorescence emission spectra were recorded from 295 nm to 420 nm upon excitation at 280 nm (2.5/5 nm bandpass for excitation and emission). Unless stated otherwise, all measurements were performed in 10 mM Hepes, pH 7.40 (EcTRP), or 50 mM sodium phosphate, pH 7.40 (hTTR), and variable concentrations of denaturant, supplied from freshly made 10 M Urea stock solutions in 10 mM Hepes, pH 7.40.

Equilibrium unfolding experiments. Equilibrium unfolding transitions were monitored by changes in Trp fluorescence and were rendered from scanned fluorescence emission spectra by calculating the ratio of fluorescence emission intensity at 360 nm and 325 nm (360/325 nm, EcTRP) or 355 nm and 335 nm (355/335 nm, TTR). Individual protein samples (1.5 μM tetramer) that varied in denaturant concentration were prepared and incubated at 25 °C until equilibrium was reached. Because EcTRP and hTTR are tetrameric proteins, their thermodynamic stability is concentration dependent. In this work, no effort is made to extract accurate free energies, and unfolding transitions were measured at a single protein concentration (1.50 μM tetramer) and are represented as transitions normalized to the fraction of folded protein.

Kinetic experiments. Protein unfolding kinetics that was complete within 24 h was collected in real time in a fluorimeter equipped with a four-cell holder, or an eight-cell holder turret wheel. The temperature was set to 25 °C using a Peltier element. For slower unfolding kinetics, direct measurements of the kinetics were not practicable. Unfolding trajectories were thus collected in interrupted mode, as described previously for TTR. In brief, fluorescence emission scans were collected at individual time points upon mixing with surfactant or denaturant, and the unfolding trajectory was rendered from the scanned spectra by calculating and plotting the fluorescence ratio at two wavelengths as described in the previous section. Using a ratio of intensities rather than intensities at a single wavelength was found necessary, as the sample cuvette had to be removed and reinserted between measurements. Moving the cuvette causes minor fluctuations in intensities that are eliminated by using a fluorescence emission ratio, which is sensitive to spectral shifts but not variation in intensities. For each unfolding experiment and buffer conditions, typically 10 to 15 appropriately spaced emission spectra were recorded.

Kinetic data are represented as plots of the log-transformed rate constant for unfolding (ln(ku)) vs. denaturant or denaturant–surfactant (dodine) concentration. For proteins that obey two-state folding, the measured rate constants are the sum of individual microscopic rate constants for folding and unfolding ($k_{obs} = k_f + k_u$). In this study, we are interested in the rates of unfolding and the associated free energy barriers. We thus limit ourselves to denaturant concentrations where the contributions from refolding processes to the observed rate constant is minimal, such that the measured rate constant approximates the microscopic unfolding rate constant ($k_{obs} = k_u$). This condition is met by using denaturant concentrations where the fraction of unfolded protein under equilibrium conditions is >0.80.

Dodine measurements. Dodine (acetate salt) was purchased in bottles of 250 mg (nominal weight) lyophilized powder. Seven mL ethanol (100%) was added to each bottle. The solution was heated at 60 °C in a water bath under occasional shaking to fully dissolve the powder. The dodine stock solution (124.5 mM nominal concentration) was aliquoted into screw-cap tubes and stored at −80 °C until use. Immediately prior to use, the surfactant that precipitated upon cold storage was resolubilized by heating the sealed tube in a water bath at 60 °C. As reported by Gruebele and coworkers, dodine solubility is negatively affected by salt ions, and phosphate ions in particular. No aggregation of dodine is observed in 10 mM Hepes, pH 7.4 (titrated with NaOH), up to a concentration of at least 8 mM dodine, or in the presence of Urea as cosolvent up to a concentration of 10 M.

The CMC of dodine in 10 mM Hepes, pH 7.40, was estimated by using a lipophilic cyanine-based dye (3,3′-dioctadecyloxacarbocyanine perchlorate or DiO hereafter) as a reporter fluorophore (39). Fluorescence emission spectra of DiO (1.5 μM) were recorded at dodine concentrations ranging from 0 to 7 mM. In low-salt, aqueous solution, DiO is basically nonfluorescent. The onset of dodine micelle formation can be inferred from an increase in DiO fluorescence, as the lipid-soluble dye will partition into micelles. In this text, and consistent with common practice in the field, we define the CMC of dodine as the concentration where linear fits to the flat and steep portion of the plot of DiO fluorescence vs. surfactant concentration intersect. We estimate a CMC of 3.5 mM for dodine in 10 mM Hepes, pH 7.40. This value is consistent with the CMC's reported for dodine in earlier work. To ascertain conditions where dodine is present in nonmicellar form, and to avoid possible kinetic heterogeneity due to the coexistence of micelles, all thermodynamic and kinetic data on EcTRP were collected at dodine concentrations below 4 mM.

For equilibrium unfolding experiments with dodine, individual protein samples (1.5 μM tetramer and 0 to 7 mM dodine) were incubated for 3 to 12 d at 25 °C. Normalized equilibrium unfolding transitions were rendered from scanned fluorescence emission spectra, as described for chemical denaturants in the previous paragraph.

As dodine cooperatively unfolds EcTRP in the absence of denaturant, dodine can be used to study the unfolding kinetics of EcTRP at conditions that are not accessible by chemical denaturant (for EcTRP, below 3 M urea). We found that dodine accelerates EcTRP unfolding in a concentration-dependent manner. The log-transformed unfolding rate [$\ln(k_u)$] increases approximately linearly with

dodine concentration up to a concentration of at least 3 mM. To account for the accelerating effect of dodine on unfolding kinetics, and to obtain corrected unfolding rate constants, we used the method of linear extrapolation, which is well established to correct rates measured in chemical denaturants. Briefly, at each buffer condition (e.g., 1 M Urea), unfolding experiments were performed at several dodine concentrations (1.5 to 3.5 μM). The resulting unfolding trajectories were fit to a single exponential and the log-transformed unfolding rate constant is plotted against the dodine concentration. A linear fit to the data yields the corrected rate under the conditions used (e.g., 1 M urea).

CD Experiment. CD spectra were measured in a Jasco J-1500 spectropolarimeter at 25 °C. For near-UV CD spectra, measurements were made in a 1 cm pathlength quartz cuvette. Spectra were scanned from 250 to 315 nm at 0.2 nm resolution. The protein concentration was 12.7 μM tetramer (corresponding to an absorbance of 1.0 at 280 nm) in 10 mM Hepes, pH 7.40. Spectra were scanned both in the absence of dodine (folded protein) or in the presence of 3 mM dodine (dodine-denatured state). The same solution was also used for recording far-UV CD spectra (185 to 250 nm), but measurements were made in 0.1 mm quartz capillary force cells (Jasco Inc.) to minimize background contributions to the spectra from solvent below 200 nm. To record reference far- and near-UV CD spectra of pH-denatured EcTRP, the protein was extensively dialyzed against water adjusted to pH 2 using hydrochloride acid. Consistent with earlier reports, EcTRP remained fully soluble under these acidic conditions. Reported spectra were rendered from unprocessed raw spectra using an averaging window of five data points and were converted into units of molar ellipticities.

Small-Molecule Ligand-Binding Assay. The ligand-binding activity of hTTR and TRP/TTR hybrids was studied using a covalent modification assay, as described previously. Native hTTR or TRP/TTR hybrid tetramer (2 μM) was reacted with a stoichiometric excess of reactive stilbene ***A2*** (20 μM, administered from a 5 mM stock solution in DMSO) that is covalently modified by pKa-perturbed Lys15 in the native tetramer to create an ***A2***-TTR adduct with bright blue fluorescence. ***A2*** activation was monitored in a fluorimeter at 25 °C by following the increase in ***A2*** fluorescence emission intensity at 428 nm (excitation: 330 nm) over time.

Data, Materials, and Software Availability. All study data are included in the article and/or *SI Appendix*.

ACKNOWLEDGMENTS. This work was supported by NSF grant MCB 2205665 (M.G.) and NIH DK 046335 (M.J. and J.W.K.). Editorial support was provided by Dr. Emily P. Bentley. This is manuscript #30262 from The Scripps Research Institute.

1. T. Eneqvist, E. Lundberg, L. Nilsson, R. Abagyan, A. E. Sauer-Eriksson, The transthyretin-related protein family. *Eur. J. Biochem.* **270**, 518–532 (2003).
2. E. Lundberg, S. Bäckström, U. H. Sauer, A. E. Sauer-Eriksson, The transthyretin-related protein: Structural investigation of a novel protein family. *J. Struct. Biol.* **155**, 445–457 (2006).
3. L. Cendron *et al.*, Probing the evolution of hydroxyisourate hydrolase into transthyretin through active-site redesign. *J. Mol. Biol.* **409**, 504–512 (2011).
4. S. J. Richardson, Tweaking the structure to radically change the function: The evolution of transthyretin from 5-hydroxyisourate hydrolase to triiodothyronine distributor to thyroxine distributor. *Front. Endocrinol.* **5**, 245 (2015).
5. S. J. Richardson, Evolutionary changes to transthyretin: Evolution of transthyretin biosynthesis: Evolution of transthyretin biosynthesis. *FEBS J.* **276**, 5342–5356 (2009).
6. L. Carrijo De Oliveira *et al.*, Reenacting the birth of a function: Functional divergence of HIUases and transthyretins as inferred by evolutionary and biophysical studies. *J. Mol. Evol.* **89**, 370–383 (2021).
7. P. Hammarström, R. L. Wiseman, E. T. Powers, J. W. Kelly, Prevention of transthyretin amyloid disease by changing protein misfolding energetics. *Science* **299**, 713–716 (2003).
8. A. Quintas, M. J. M. Saraiva, R. M. M. Brito, The tetrameric protein transthyretin dissociates to a non-native monomer in solution. *J. Biol. Chem.* **274**, 32943–32949 (1999).
9. S. M. Johnson, S. Connelly, C. Fearns, E. T. Powers, J. W. Kelly, The transthyretin amyloidoses: From delineating the molecular mechanism of aggregation linked to pathology to a regulatory-agency-approved drug. *J. Mol. Biol.* **421**, 185–203 (2012).
10. W. Colon, J. W. Kelly, Partial denaturation of transthyretin is sufficient for amyloid fibril formation in vitro. *Biochemistry* **31**, 8654–8660 (1992).
11. Z. Lai, W. Colón, J. W. Kelly, The acid-mediated denaturation pathway of transthyretin yields a conformational intermediate that can self-assemble into amyloid. *Biochemistry* **35**, 6470–6482 (1996).
12. M. Manning, W. Colón, Structural basis of protein kinetic stability: Resistance to sodium dodecyl sulfate suggests a central role for rigidity and a bias toward β-sheet structure. *Biochemistry* **43**, 11248–11254 (2004).
13. I. Rappley *et al.*, Quantification of transthyretin kinetic stability in human plasma using subunit exchange. *Biochemistry* **53**, 1993–2006 (2014).
14. R. L. Wiseman, E. T. Powers, J. W. Kelly, Partitioning conformational intermediates between competing refolding and aggregation pathways: Insights into transthyretin amyloid disease. *Biochemistry* **44**, 16612–16623 (2005).
15. A. R. Hurshman Babbes, E. T. Powers, J. W. Kelly, Quantification of the thermodynamically linked quaternary and tertiary structural stabilities of transthyretin and its disease-associated variants: The relationship between stability and amyloidosis. *Biochemistry* **47**, 6969–6984 (2008).
16. E. Lundberg, A. Olofsson, G. T. Westermark, A. E. Sauer-Eriksson, Stability and fibril formation properties of human and fish transthyretin, and of the Escherichia coli transthyretin-related protein: Stability and fibril formation of TTR and TRP. *FEBS J.* **276**, 1999–2011 (2009).
17. S. D. Santos *et al.*, Amyloidogenic properties of transthyretin-like protein (TLP) from *Escherichia coli*. *FEBS Lett.* **582**, 2893–2898 (2008).
18. D. U. Ferreiro, E. A. Komives, P. G. Wolynes, Frustration in biomolecules. *Q. Rev. Biophys.* **47**, 285–363 (2014).
19. M. Jäger *et al.*, Structure-function-folding relationship in a WW domain. *Proc. Natl. Acad. Sci. U.S.A.* **103**, 10648–10653 (2006).
20. Y. Guan, Z. Wang, A. Cao, L. Lai, X. S. Zhao, Subunit exchange of MjHsp16.5 studied by single-molecule imaging and fluorescence resonance energy transfer. *J. Am. Chem. Soc.* **128**, 7203–7208 (2006).
21. R. L. Wiseman, N. S. Green, J. W. Kelly, Kinetic stabilization of an oligomeric protein under physiological conditions demonstrated by a lack of subunit exchange: Implications for transthyretin amyloidosis. *Biochemistry* **44**, 9265–9274 (2005).
22. F. Schneider, P. Hammarström, J. W. Kelly, Transthyretin slowly exchanges subunits under physiological conditions: A convenient chromatographic method to study subunit exchange in oligomeric proteins. *Protein Sci.* **10**, 1606–1613 (2001).
23. K. Xia *et al.*, Identifying the subproteome of kinetically stable proteins via diagonal 2D SDS/PAGE. *Proc. Natl. Acad. Sci. U.S.A.* **104**, 17329–17334 (2007).
24. K. Xia *et al.*, Quantifying the kinetic stability of hyperstable proteins via time-dependent SDS trapping. *Biochemistry* **51**, 100–107 (2012).
25. H. Gelman, T. Perlova, M. Gruebele, Dodine as a protein denaturant: The best of two worlds? *J. Phys. Chem. B* **117**, 13090–13097 (2013).
26. D. Guin, K. Sye, K. Dave, M. Gruebele, Dodine as a transparent protein denaturant for circular dichroism and infrared studies. *Protein Sci.* **25**, 1061–1068 (2016).
27. D. Guin, S. Mittal, B. Bozymski, D. Shukla, M. Gruebele, Dodine as a Kosmo-chaotropic agent. *J. Phys. Chem. Lett.* **10**, 2600–2605 (2019).
28. B. Biswas, P. C. Singh, Does fungicide "dodine" unfold protein like Kosmo-chaotropic agent? *J. Phys. Chem. B* **123**, 8240–8246 (2019).
29. J. Huang, T. D. Craggs, J. Christodoulou, S. E. Jackson, Stable intermediate states and high energy barriers in the unfolding of GFP. *J. Mol. Biol.* **370**, 356–371 (2007).
30. A. Hörnberg, T. Eneqvist, A. Olofsson, E. Lundgren, A. E. Sauer-Eriksson, A comparative analysis of 23 structures of the amyloidogenic protein transthyretin. *J. Mol. Biol.* **302**, 649–669 (2000).
31. T. R. Foss, R. L. Wiseman, J. W. Kelly, The pathway by which the tetrameric protein transthyretin dissociates. *Biochemistry* **44**, 15525–15533 (2005).
32. S. Zhou, H. Zou, Y. Wang, G. V. Lo, S. Yuan, Atomic mechanisms of transthyretin tetramer dissociation studied by molecular dynamics simulations. *J. Chem. Inf. Model.* **62**, 6667–6678 (2022).
33. J. Zhang *et al.*, Structure-based virtual screening protocol for *in silico* identification of potential thyroid disrupting chemicals targeting transthyretin. *Environ. Sci. Technol.* **50**, 11984–11993 (2016).
34. R. G. Manzon, T. M. Neuls, L. A. Manzon, Molecular cloning, tissue distribution, and developmental expression of lamprey transthyretins. *Gen. Comp. Endocrinol.* **151**, 55–65 (2007).
35. L. Kollipara, R. P. Zahedi, Protein carbamylation: In vivo modification or in vitro artefact? *Proteomics* **13**, 941–944 (2013).
36. A. Hörnberg, U. W. Hultdin, A. Olofsson, A. E. Sauer-Eriksson, The effect of iodide and chloride on transthyretin structure and stability. *Biochemistry* **44**, 9290–9299 (2005).
37. K. Yamauchi, K. Kasai, Sequential molecular events of functional trade-offs in 5-hydroxyisourate hydrolase before and after gene duplication led to the evolution of transthyretin during chordate diversification. *J. Mol. Evol.* **86**, 457–469 (2018).
38. K. Matsubara, M. Mizuguchi, K. Kawano, Expression of a synthetic gene encoding human transthyretin in Escherichia coli. *Protein Expr. Purif.* **30**, 55–61 (2003).
39. A. M. Peterson, Z. Tan, E. M. Kimbrough, J. M. Heemstra, 3,3′-Dioctadecyloxacarbocyanine perchlorate (DiO) as a fluorogenic probe for measurement of critical micelle concentration. *Anal. Methods* **7**, 6877–6882 (2015).